doi:10.1016/j.jmb.2009.02.001 *J. Mol. Biol.* (2009) **387**, 607–618

JMB

Available online at www.sciencedirect.com

ScienceDirect

ELSEVIER

Shared Catalysis in Virus Entry and Bacterial Cell Wall Depolymerization

Daniel N. Cohen[1,2], Yuk Y. Sham[3], Greg D. Haugstad[4], Ye Xiang[5], Michael G. Rossmann[5], Dwight L. Anderson[1,2,6] and David L. Popham[7]*

[1]*Department of Microbiology, Medical School, University of Minnesota, Minneapolis, MN 55455, USA*

[2]*Institute for Molecular Virology, University of Minnesota, Minneapolis, MN 55455, USA*

[3]*Center for Drug Design, University of Minnesota, Minneapolis, MN 55455, USA*

[4]*Department of Physics, Characterization Facility, Institute of Technology, University of Minnesota, Minneapolis, MN 55455, USA*

[5]*Department of Biological Sciences, Purdue University, West Lafayette, IN 47907, USA*

[6]*Department of Diagnostic and Biological Sciences, School of Dentistry, University of Minnesota, Minneapolis, MN 55455, USA*

[7]*Department of Biological Sciences, Virginia Tech, Blacksburg, VA 24061, USA*

Received 4 November 2008; received in revised form 31 January 2009; accepted 2 February 2009
Available online 9 February 2009

Edited by M. Guss

Bacterial virus entry and cell wall depolymerization require the breakdown of peptidoglycan (PG), the peptide-cross-linked polysaccharide matrix that surrounds bacterial cells. Structural studies of lysostaphin, a PG lytic enzyme (autolysin), have suggested that residues in the active site facilitate hydrolysis, but a clear mechanism for this reaction has remained unsolved. The active-site residues and a structural pattern of β-sheets are conserved among lysostaphin homologs (such as LytM of *Staphylococcus aureus*) and the C-terminal domain of gene product 13 (gp13), a protein at the tail tip of the *Bacillus subtilis* bacteriophage ϕ29. gp13 activity on PG and muropeptides was assayed using high-performance liquid chromatography, and gp13 was found to be a D,D-endopeptidase that cleaved the peptide cross-link. Computational modeling of the *B. subtilis* cross-linked peptide into the gp13 active site suggested that Asp195 may facilitate scissile-bond activation and that His247 is oriented to mediate nucleophile generation. To our knowledge, this is the first model of a Zn^{2+} metallopeptidase and its substrate. Residue Asp195 of gp13 was found to be critical for Zn^{2+} binding and catalysis by substitution mutagenesis with Ala or Cys. Circular dichroism and particle-induced X-ray emission spectroscopy showed that the general protein folding and Zn^{2+} binding were maintained in the Cys mutant but reduced in the Ala mutant. These findings together support a model in which the Asp195 and His247 in gp13 and homologous residues in the LytM and lysostaphin active sites facilitate hydrolysis of the peptide substrate that cross-links PG. Thus, these autolysins and phage-entry enzymes have a shared chemical mechanism of action.

Keywords: bacteriophage; metallopeptidase; autolysin; ϕ29; gp13

**Corresponding author.* E-mail address: dpopham@vt.edu.

Present address: D. N. Cohen, Medical Scientist Training Program, Vanderbilt University School of Medicine, Nashville, TN 37232, USA.

Abbreviations used: NTD, amino-terminal domain; CTD, carboxy-terminal domain; Dpm, diaminopimelic acid; gp, gene product; NAM, *N*-acetylmuramic acid; NAG, *N*-acetylglucosamine; PIXE, particle-induced X-ray emission; PG, peptidoglycan; *sus*, suppressor-sensitive; wt, wild-type; FDNB, fluorodinitrobenzene.

Introduction

Bacterial cell growth and infection by bacteriophages require depolymerization of the peptidoglycan (PG) cell wall. Autolysis is the process of cell wall degradation by self-produced enzymes that normally permit bacterial cell expansion and division. Phages are extremely efficient at crossing the cell wall barrier during infection by both mechanical (phages T4 and P22)[1–3] and enzymatic (phages GA-1, ϕ29, K1E, K1-5, P22, PRD1, T4, T5, and T7/T3)[4–11] means. The latter involves a battery of lysozymes, amidases, transglycosylases, and endopeptidases that cleave either the polysaccharide or peptide bonds of the PG, providing access to the lipid bilayer. The PG of *Bacillus subtilis*, the host of bacteriophage ϕ29, is depicted in Fig. 1a.

Structural and biochemical studies have enlightened autolysin-mediated PG depolymerization for cell division and lysozyme-mediated phage entry into host bacteria. Atomic structures are available for both the inactive[13] and active[14] forms of the Zn^{2+} metallopeptidase LytM of *Staphylococcus aureus*, a homolog of the lysostaphin of *Staphylococcus simulans*. Lysostaphin is a well-studied metallopeptidase that cleaves the pentaglycine cross-link of the staphylococcal cell wall during autolysis.[15–20] The atomic structures of the lysostaphin homolog Ale-1 of *Staphylococcus capitis*[21] and LAS protein MepA of *Escherichia coli*[22] have also been determined. However, the precise molecular mechanism for catalysis by the conserved amino acids within LytM, lysostaphin, and the lysostaphin-like enzymes remains unknown.[15,19] Models and co-crystallized structures of lysostaphin-like peptidases with bound substrates are also not available. Sequence alignments have suggested the presence of lysostaphin-like homologs in phages of *B. subtilis*[23] and *Lactobacillus*,[24] and these are virion components. However, biochemical characterization of these phage proteins has not confirmed the proposed activity.

Bacteriophage ϕ29 has served as a model for virus assembly mechanisms.[25,26] Early studies of the ϕ29 interaction with the host cell wall revealed that glucosylated teichoic acids, rather than a protein,

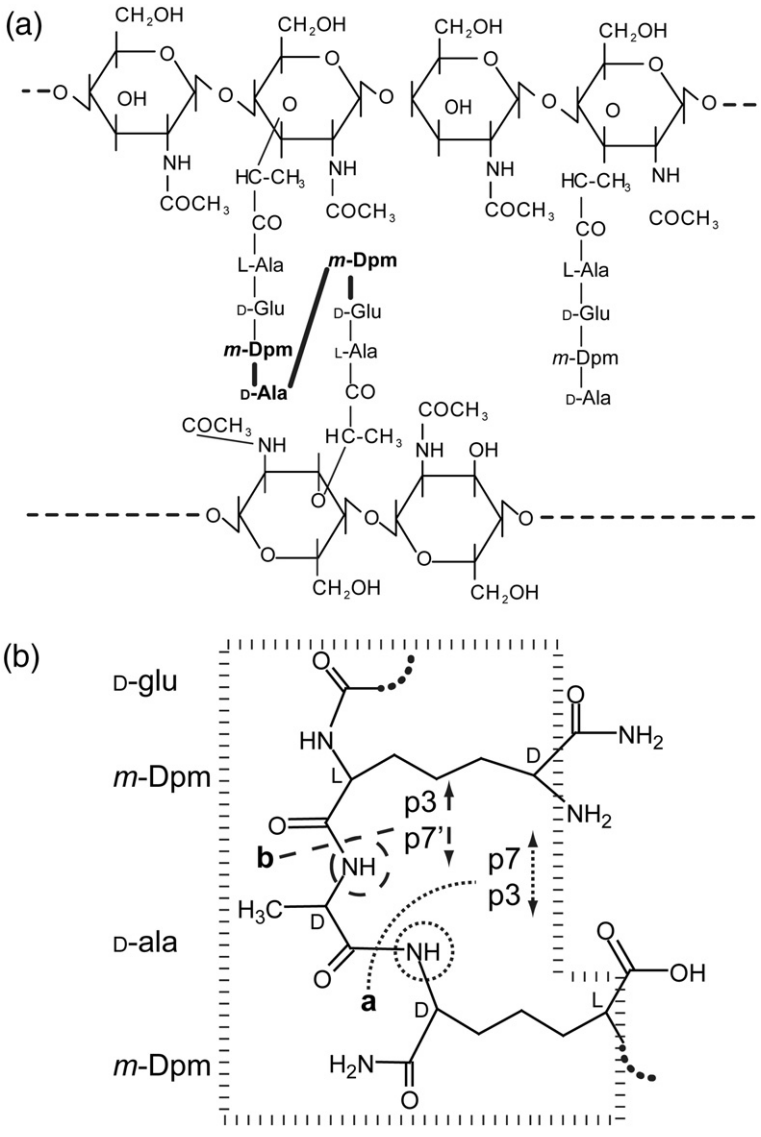

Fig. 1. *B. subtilis* cell wall PG structures. (a) *B. subtilis* cell wall PG is composed of alternating NAG and NAM residues with peptide side chains. Peptides can be cross-linked via the D-Ala in position 4 and the free ε-amino group of Dpm. More than 95% of the Dpm free carboxylate groups are amidated.[12] The predominant cross-linked muropeptide fragment, p21, is two disaccharides cross-linked as shown via their peptide side chains [panel (a), left]. The activity of gp13 cleaves p21 to produce a disaccharide tripeptide and a disaccharide tetrapeptide. This could result from hydrolysis of either of two bonds [panel (b), sites a and b] surrounding the cross-link [panel (a), bold amino acids and bonds]. However, the potential disaccharide-tetrapeptide products differ in the amino acids that have free amino groups [panel (b), circles] and thus can be differentiated after modification of these amino groups followed by amino acid analysis (Table 1). The cross-link fragment used for modeling is shown, and the chiral centers are indicated as "L" or "D" [panel (b), dashed box].

serve as the receptor.[27,28] Furthermore, the ability of the phage to adsorb to teichoic acids has been shown to reside in the phage tail appendages.[29] However, adsorption alone is insufficient for infection and progeny production; successful puncture of the cell wall is also required. Here, biochemical study of the cell wall-depolymerizing metallopeptidase of bacteriophage ϕ29 of *B. subtilis*, gene product 13 (gp13), a homolog of the *S. aureus* autolysin LytM, is complemented by computational modeling. A possible mechanism of the unified action of phage-entry enzymes and autolysins is proposed based on biochemical and computational characterization of the phage ϕ29 morphogenetic factor/cell wall-depolymerizing enzyme gp13.[23,30]

Results

Purified ϕ29 particles and gp13 cleave the *B. subtilis* PG cross-links

Previous studies localized gp13 to the distal ϕ29 tail, the site of DNA injection following host cell binding, by immuno-electron microscopy[23] and cryo-electron microscopy.[31] A β-sheet-rich C-terminal domain (CTD) of gp13[23,31] is similar to LytM, the lysostaphin homolog in *S. aureus*, while the N-terminal domain (NTD) is α-helix rich.

To test the activity of ϕ29 on the purified PG of *B. subtilis* (Fig. 1a), we pseudo-infected purified cell wall sacculi with wild-type (wt) ϕ29 (see Methods). It is estimated that there are hundreds of glucosylated teichoic acid ϕ29 receptors per bacterium,[27] and each cell has been shown to adsorb ~400 ϕ29 particles.[29] Intact PG was largely insoluble and could be pelleted for subsequent muramidase solubilization (see Methods) and high-pressure liquid chromatography (HPLC) analysis of muropeptides from the pelleted PG. Following pseudo-infection of sacculi with ϕ29, there was release of muropeptides, predominantly p7 (Supplementary Fig. 1d), a disaccharide-tetrapeptide component of the *B. subtilis* PG (Fig. 1b), into the supernatant, while intact PG had little soluble material (Supplementary Fig. 1b). There was also a modest decrease in the cross-linked muropeptide p21 in the ϕ29-treated insoluble fraction (Supplementary Fig. 1c) compared with the untreated control PG (Supplementary Fig. 1a).

Incubation of sacculi (Fig. 2, blue trace) with purified gp13 (Fig. 2, red trace; offset by 1 min) also revealed a modest decrease in cross-linked species with a corresponding increase in un-cross-linked species. gp13 did not cause cleavage of pentaglycine, the lysostaphin substrate in a thin-layer chromatography assay often used for lysostaphin study[13] (data not shown).

To ensure that gp13 was a tail component with enzymatic activity, we employed HPLC tracking of the dominant cross-linked muropeptide p21 with ϕ29 virions and gp13 (Fig. 3a). Incubation of ϕ29 with purified p21 resulted in modest cleavage of p21 to products of smaller molecular mass (Fig. 3a, bottom red line), visualized most clearly on subtraction of the baseline absorption from the raw traces of particles incubated with p21 (Supplementary Fig. 2). Product peaks are at ~15 and ~30 min (Fig. 3a). The precursor prohead particle, which lacks gp13, does not show the 15- or 30-min peaks (Fig. 3a, bottom black line). This subtle difference suggested that gp13 of the virion tail may have catalytic activity.

Purified cross-linked species were utilized to determine if gp13 contained the enzymatic activity on p21 observed with the virion. gp13 cleaved p21 to products that co-migrated with the ϕ29 products (Fig. 3a, top black line). p15, p21, p22, and p23 (Fig. 3b) are various forms of the cross-linked muropeptide group.[12] p21, the predominant form, is acetylated on both glucosamine residues (Fig. 1a), while p22 and p23 are deacetylated on one of the two glucosamine residues and p15 is amidated on only one of the diaminopimelic acid (Dpm) residues. gp13 incubated with each purified cross-linked muropeptide showed substantial product formation (Fig. 3b)

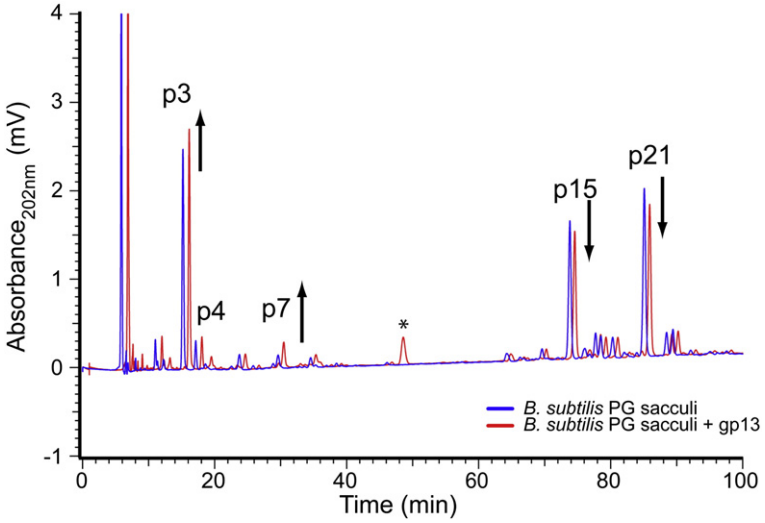

Fig. 2. gp13 activity on purified *B. subtilis* PG. Mutanolysin digestion of *B. subtilis* sacculi produces a characteristic profile of peaks (blue line). The untreated sacculi (blue) show the characteristic pattern of cross-linked (>60 min) and un-cross-linked (<40 min) muropeptides. Following incubation with purified gp13 protein, a modest increase in monomer disaccharide (DS) tripeptide (TriP) and DS tetrapeptide (TP) peaks (<40 min) is apparent with a slight decrease in cross-linked peaks beyond 60 min (red line). The 43.5-min peak present in the gp13 sample (*, red line) is a contaminant from the purified protein solution.

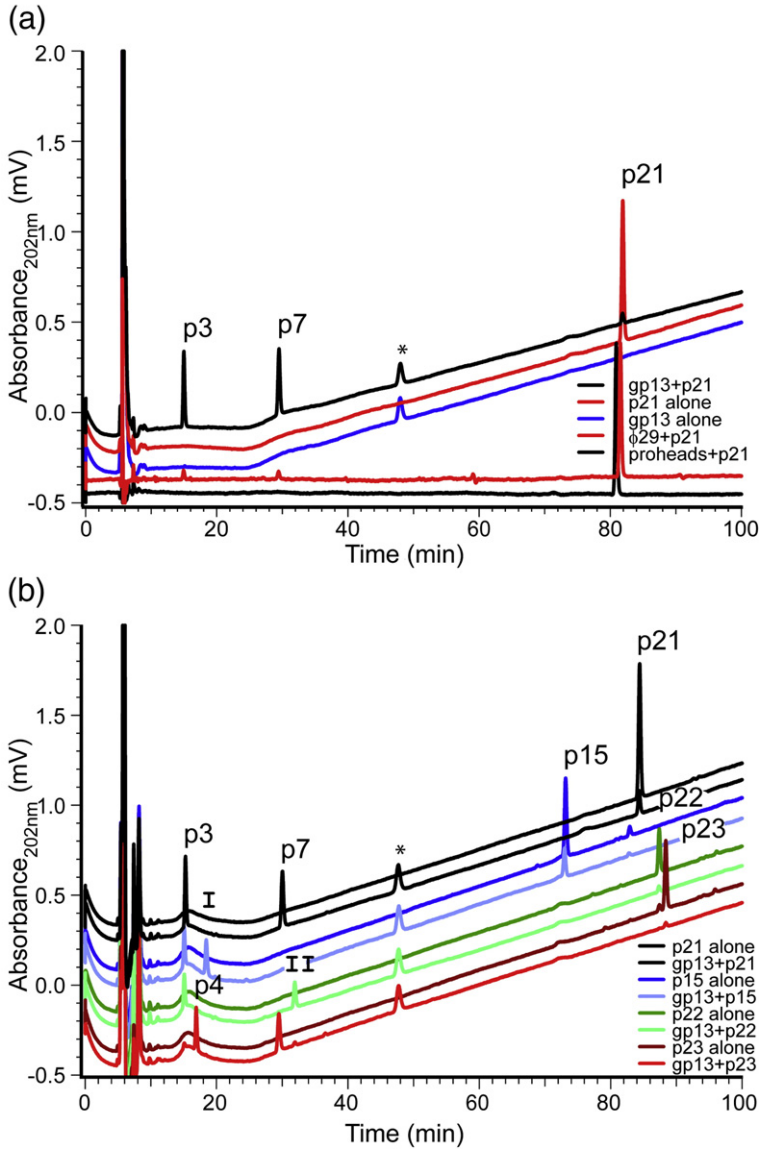

Fig. 3. Purified gp13 and ϕ29 cleaved p21 to the same products, and this activity functions on p15, p22, and p23. Purified p21 alone (a, top red) shows a lone peak at ~81 min, while purified gp13 alone (a, blue) lacks the 81-min peak but contains a 49-min contaminant (*). Incubation of gp13 with p21 (a, top black) shows reduction of p21, with the appearance of two product peaks at 15 and 30 min. These peaks are present on p21 incubation with ϕ29 (a, bottom red) but not with gp13-lacking proheads (a, bottom black). These latter two lines are flat because they were produced by subtractions of background runs (Supplementary Fig. 2). (b) Deacetylated (deacetyl) and amidated (amid) forms of the cross-linked muropeptide of *B. subtilis* are all cleaved to lower-molecular-weight products. p3, DS-TriP^{Amid}; p4, DS^{Deacetyl}-TriP^{Amid}; p7, DS-TP^{Amid}; p15, DS-TriP^{Amid}-TP-DS; p21, DS-TriP^{Amid}-TP^{Amid}-DS; p22, DS-TriP^{Amid}-TP^{Amid}-DS^{Deacetyl}; p23, DS^{Deacetyl}-TriP^{Amid}-TP^{Amid}-DS; I, DS-TP; and II, DS^{Deacetyl}-TP^{Amid}.

to species that migrated at ~15 and ~30 min. These products had elution times consistent with those of previously identified muropeptides[12,32] (Supplementary Fig. 1a).

ϕ29 and gp13 cleave the site of the original peptide cross-link formation

Cleavage of the cross-linked peptides may occur at a number of sites: two are illustrated here (Fig. 1b). Mass spectrometry analysis of the peak contents that eluted at 15 and 30 min demonstrated masses consistent with p3 and p7 (Fig. 1b, site a) and with p3 and p7′ (Fig. 1b, site b) (Table 1). Fluorodinitrobenzene (FDNB) modification of free amino groups in the cleavage products, followed by amino acid analysis, was used to differentiate p7 from p7′ and to determine the specific cleavage site of gp13. p7 and p3 (Fig. 1b, site a) are the products of p21 cleavage by gp13, because only Dpm reacted with FDNB (Table 1).

Table 1. Muropeptide structure analyses

Muropeptide name	Muropeptide structure	m/z (M−H)$^-$		Amino acid analysis (molar ratios)					
				−FDNB			+FDNB		
		Predicted	Observed	Ala	Dpm	Glu[a]	Ala	Dpm	Glu[a]
p21	DS-TP-DS-TriP	1790.8	1790.6	1.6	1.1	1	1.5	0.5	1
p3	DS-TriP	868.9	868.3	1.1	0.9	1	1.0	0.0	1
p7	DS-TP	939.4	939.3	2.0	1.1	1	1.5	0.1	1

DS indicates disaccharide; TP, tetrapeptide; TriP, tripeptide.
[a] Glu was set to 1 for calculation of molar ratios.

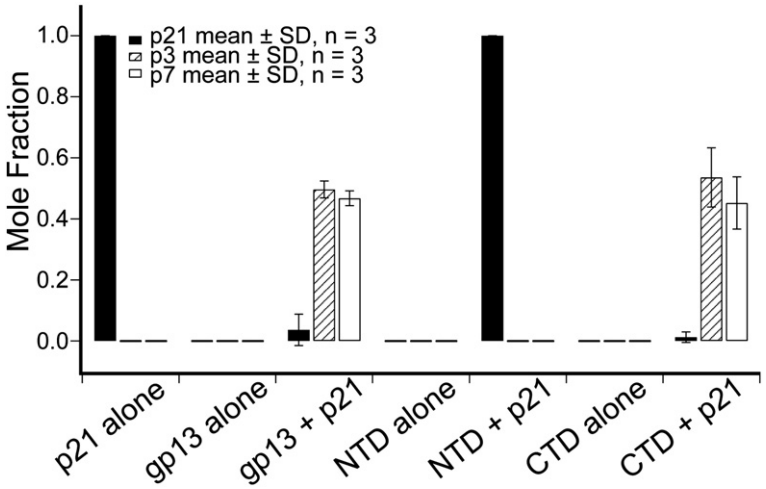

Fig. 4. Domain specificity of gp13-mediated cross-link cleavage. Mass-corrected peak area from HPLC analysis of purified NTD and CTD of gp13 incubated with p21. p21 remained uncleaved with the NTD, while product formation was nearly complete with the CTD. p21 is represented by solid bars; p3, by hatched bars; and p7, by open bars.

Alanine would have reacted with FDNB if p7′ had been the other product (Fig. 1b, site b).

Preliminary assessment of product formation kinetics (Supplementary Fig. 3) suggested that the gp13 solution cleavage rate is slow (~1–2/min); however, a similar rate reported for the phage P22 tail spike endorhamnosidase gp9[33] is sufficient for infection.

The CTD of gp13 is active on the PG cross-link

Predictions in previous work[23,31] suggested that the gp13 CTD may contain the enzymatic activity on the PG cross-link. To determine if the CTD contains the cross-link-cleaving activity of the protein, we expressed the NTD and CTD separately and purified and tested for their activity in the HPLC assay on the cross-linked muropeptide p21. The NTD is 159 aa in length and 18.4 kDa in mass, while the CTD is 202 aa in length and 22.3 kDa in mass (wt gp13 is 365 aa in length and 40.9 kDa in mass) (calculated using ExPASy ProtParam[34]). The mole fractions of the substrate and products are shown for the CTD and NTD alone compared with full-length gp13 (Fig. 4). p3 and p7 were produced by the CTD but not by the NTD.

Computational modeling of the gp13-muropeptide complex shows the orientation of the scissile bond

To elucidate the catalytic mechanism underlying the cross-link cleavage mediated by the gp13 CTD and therefore the autolysins, such as LytM, we modeled the central segment of the p21 muropeptide containing the Dpm-D-Ala-Dpm region (Fig. 1b, dashed box) into the putative active site of gp13. The catalytic binding site of gp13 was identified as the region enclosing the cleft of the gp13 β-sheet domain[31] containing a Zn^{2+} cofactor. This region also contains several residues that are highly conserved across LytM and gp13-like proteins of other ϕ29-related and lactococcal phages (Fig. 5). The original

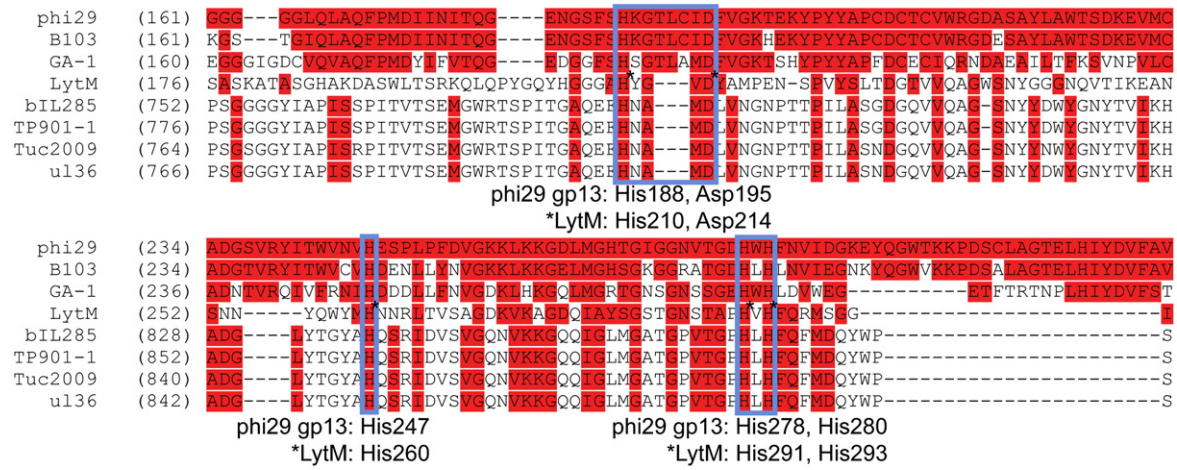

Fig. 5. Sequence alignment of gp13 in ϕ29, B103, and GA-1 with LytM and lactococcal phage homologs from bIL285, TP901-1, Tuc2009, and ul36. Sequence alignment of ϕ29 gp13 (top line) compared with other ϕ29 family members, GA-1 and B-103 (lines 2 and 3), LytM (line 4), and four lactococcal phages (lines 5–8), over the segment of gp13 containing the Zn^{2+} binding histidine motif and Asp195. The conserved Zn^{2+}-chelating residues (ϕ29 gp13: H188, D195, and H280; LytM*: H210, D214, and H293) and the two nearby histidine residues (ϕ29 gp13: H247 and H278; LytM*: H260 and H291) have been specifically labeled. The residue number for the first amino acid of each protein is listed in parentheses.

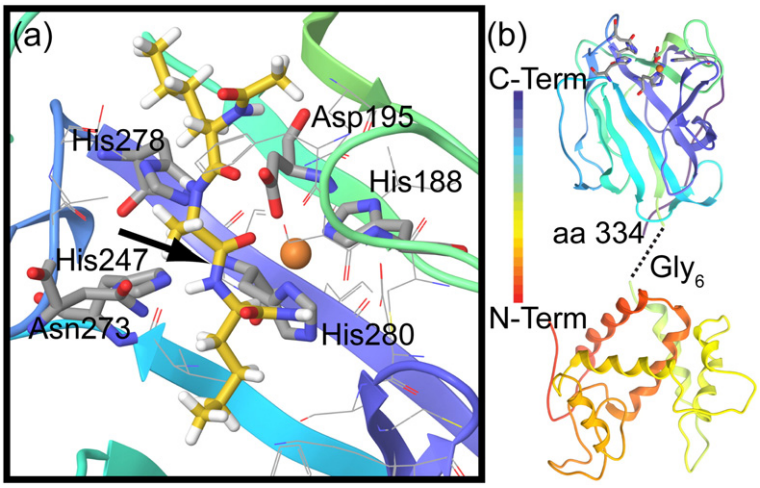

Fig. 6. Modeling of the p21 substrate cleavage target into the putative gp13 Zn^{2+}-containing active site. (a) Modeling of the p21 substrate target (carbon, yellow; oxygen, red; nitrogen, blue; hydrogen, white) containing the peptide bonds of Dpm-Ala-Dpm resulted in energy minimizations that favor orientation of the carbonyl group adjacent to the scissile bond (arrow) as the fourth Zn^{2+} ligand in gp13. All residues within 5 Å of the model fragment are shown (sticks) with six essential residues as rods. (b) The entire gp13 crystal structure is shown as a ribbon diagram for reference.

X-ray structure of apo gp13 contains a Zn^{2+} ion tetracoordinated to D195, H188, H280, and a conserved crystallographic water molecule. The closest oxygen of aspartate 195 (D195) of gp13 is 1.94 Å from Zn^{2+}, and the other oxygen is 2.87 Å from Zn^{2+}. Successful docking of the modeled substrate requires the removal of the zinc-bound crystallographic water molecule. Of the 50,000 conformations searched, only 7 poses were found, all of which shared a common mode of binding involving the carbonyl oxygen atom of the scissile amide bond positioned within 2.1–2.4 Å adjacent to the Zn^{2+} ion at the original crystallographic water site (Fig. 6a, arrow). The pose with the best docking score is reported here, and the overall model suggests the requirement of water displacement by the potential substrate from the Zn^{2+} ion as well as chelation of the carbonyl oxygen atom to Zn^{2+} ion during substrate binding. This mode of binding is supported by a previously solved X-ray structure of latent LytM of *S. aureus*, which showed the Zn^{2+} ion chelated directly to the carbonyl oxygen atom of the N117 side chain.[13] In comparison with the hydrolytic mechanism of another mononuclear zinc metallopeptidase,[20,35] the placement of the carbonyl oxygen atom adjacent to the Zn^{2+} ion is necessary in the activation of the scissile peptide bond during hydrolysis and the subsequent stabilization of the oxyanion atom of the tetrahedral intermediate. Based on this model, replacement of D195, which is directly chelated to the Zn^{2+} ion, is expected to alter the overall stabilization effect of the Zn^{2+} ion and hence indirectly affect the overall rate of enzymatic hydrolysis.

The active-site aspartate residue of gp13 binds Zn for polarization

To demonstrate the importance of D195 and its role as part of the catalytic site of gp13, we performed site-directed mutagenesis of the gp13 expression plasmid to generate cysteine and alanine substitutions. The cysteine substitution (D195C) would be expected to maintain Zn^{2+} binding but may be more electron withdrawing than aspartate.[36] The alanine substitution (D195A) is expected to block Zn^{2+} binding and catalytic activities. The D195C and D195A proteins did not show cleavage of p21 to p3 or p7 (Fig. 7a). Thus, D195 was important for enzyme activity.

To confirm that the D195C change did not prevent Zn^{2+} binding by gp13, we obtained particle-induced X-ray emission (PIXE) spectra of wt gp13, gp13 (D195C), and gp13 (D195A) (Fig. 7b). The similarity of the PIXE profiles of the wt and D195C proteins indicates that the D195C protein bound Zn^{2+}, while the D195A protein did not. Alanine substitution of the homologous aspartate in MepA (D120A) rendered this protein insoluble.[37] To confirm that gp13 D195A was soluble and to compare the secondary structure folding of wt gp13 with those of the D195A and D195C proteins, we employed circular dichroism (CD). CD spectra of gp13 and D195C show the same profile (Fig. 7c) (the vertical shift of D195C may be due to slight differences in protein concentration), while the D195A spectrum was characteristic of substantial disorder of the secondary structure that was absent in wt gp13 and gp13 D195C data. These results support the hypotheses that the CTD of gp13 is a PG cross-link-cleaving Zn^{2+}metalloprotease and that D195 is active in binding Zn^{2+}, which contributes to protein stability and substrate cleavage.

Discussion

Essential bacterial cell wall PG cleavage that occurs both in growth and cell division and during phage infection is enabled by Zn^{2+} metallopeptidases. Here, Zn^{2+} metallopeptidase action of the CTD of the phage ϕ29 gp13 on *B. subtilis* PG is documented, biochemical characteristics are studied, and a computational model of the enzyme-substrate complex is presented.

The ϕ29 virion and gp13 demonstrate cross-link-cleaving capacity

The formation of p3 and p7 cleavage products from the cross-link p21 by gp13 and the gp13-containing

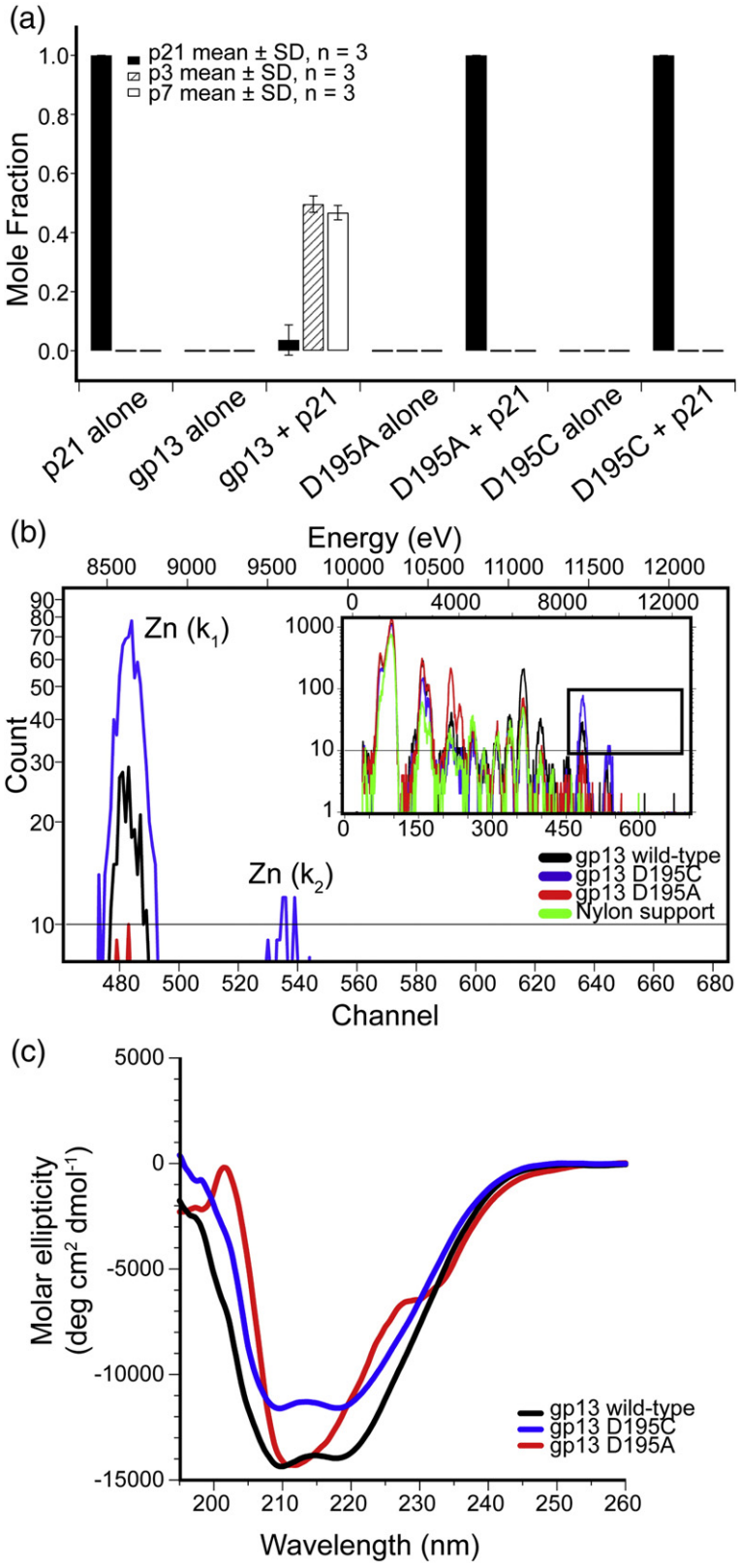

Fig. 7. gp13 aspartate 195 is involved in Zn^{2+} binding that is essential for proper protein folding and activity. (a) Mass-corrected peak area from HPLC analysis of gp13 point mutants D195C and D195A. p21 is represented by solid bars; p3, by hatched bars; and p7, by open bars. (b) PIXE spectra of wt gp13 (black) and mutants D195C (blue) and D195A (red). (c) CD of wt gp13 (black) and mutants D195C (blue) and D195A (red).

virion suggests a mechanism for ϕ29 entry and confirms the multifunctional roles of gp13.[23,30] ϕ29 gp13-defective mutant particles [*sus*13(342, 330, 53), where *sus* indicates suppressor-sensitive] are noninfectious, likely because they rapidly lose the packaged DNA[30,38] even though the gp13 fragments are in the phage[23] [*sus*13(53) contains gp13 by Western blot analysis; Supplementary Fig. 4]. In addition to this DNA retention function, the enzymatic activity of gp13 on PG cross-links (in this study) suggests that the few copies of gp13 per virion[23,31] facilitate entry of ϕ29 through the cross-linked PG layers.

The domain architecture of gp13 is similar to lysostaphin

The PG cross-link-cleaving activity of gp13 resides in the isolated CTD and is independent of the NTD (Fig. 4). In another experiment, particles of the gp13-defective mutant *sus*13(53), in which the CTD of gp13 is truncated and the NTD is intact,[23] resembled the isolated gp13 NTD; *sus*13(53) particles were unable to cleave p21 (data not shown). Activity of the CTD is also observed for the PG cross-link-cleaving enzyme LytM of *S. aureus*, in which the N-terminus is proposed to be cleaved from the precursor to produce the active enzyme.[14]

The acetylation of the cross-linked muropeptide does not affect cleavage by gp13 (Fig. 3b). The *N*-acetylglucosamine (NAG) and *N*-acetylmuramic acid (NAM) sugar residues of the PG may be expected to interact with the lysozyme-like NTD of gp13.[31] A model for enzyme activity of gp13 dimers[31] in which the NTD of one monomer, by binding the NAG–NAM substrate of the PG, aids activity and/or binding of the CTD of the other monomer to a substrate has been proposed. The absence of dependence on modifications of NAG–NAM for cross-link-cleaving activity of gp13 suggests that (1) the NTD coordination is independent of acetylation of NAG–NAM, (2) oligomers of NAM–NAG, greater than the two present in the purified muropeptides studied here, are needed for NTD binding, or (3) the NTD does not influence the CTD in a coordinated fashion as proposed.[31] An alternative model could involve the binding of the NTD of gp13 that effectively reduces the diffusion coefficient of the gp13 CTD, thereby enhancing the local cleavage of the cross-linked PG in the face of a modest catalysis rate (Supplementary Fig. 3). A similar division of target binding and catalysis between protein domains has been observed for zoocin A, a lysostaphin-like enzyme.[39]

Dual-domain enzymes are known in bacteriophages. As the dual-domain endolysins of phages B30[40] and ϕ11[41] enable progeny exit, it is of interest to know if these and other phages also have low-copy-number virion-associated entry enzymes equivalent in function to gp13 of ϕ29.

Proposed mechanism of ϕ29 entry into *B. subtilis*

Based on current observations and the literature, a model for ϕ29 entry into *B. subtilis* that includes adsorption, PG binding, lysozyme and metallopeptidase mechanisms of PG degradation, membrane puncture, and genome injection is proposed. Adsorption of the virion to glucosylated teichoic acid surrounding the PG and the likely teichoic acid cleavage by the tail appendages have been discussed previously.[42] Considering PG cross-link degradation, the CTD of gp13 may be activated much as the CTD of LytM is cleaved away from the N-terminus[14] or, alternatively, the connected NTD may aid CTD cleavage by limiting diffusion. The *in vitro* experiments presented here cannot distinguish between these *in situ* events.

After successful localized reduction in PG cross-linking, the ϕ29 tail knob gp9 may insert into the cell membrane, triggering conformational changes within the tail axis that deliver injection signals to the head–tail connector to initiate genome expulsion. A portion of genome would be propelled by pressure from the packaged DNA,[43,44] and subsequent traction of the remaining DNA would continue.[45]

Zn^{2+} polarization is essential for catalysis in lysostaphin-like enzymes

D195 of gp13 is essential for catalysis and is superimposed on the LytM aspartate 214.[23] Support for the essentiality of D195 is found in Ale-1 of *S. capitis*[46] and MepA of *E. coli*,[47] in which mutation to alanine abrogates function (Ale-1) or renders this expressed protein insoluble and inactive (MepA). However, differentiation between Zn^{2+} binding for secondary structure determination and Zn^{2+} polarization for catalysis has not been discussed in other systems. Here, PIXE demonstrated that D195 of gp13 participates as a Zn^{2+} ligand, as suggested by sequence homology[23] and the gp13 crystal structure.[31] Zn^{2+} binding was demonstrated for the Cys substitution mutant (D195C) by PIXE, but the Ala substitution mutant (D195A) showed appreciably reduced Zn^{2+} signal (Fig. 7b). Although the D195C protein binds zinc, it is inactive for structural and/or electronic reasons. These data suggest that D195 is sufficiently electronegative to facilitate catalysis. Residues in LytM, lysostaphin, Ale-1, and MepA homologous to gp13 D195 may also provide the necessary action for catalysis.

In the current model of hydrolysis by lysostaphin-like enzymes,[20] gp13-D195 would properly bind Zn^{2+}, polarizing the carbonyl carbon of the substrate for susceptibility to nucleophilic attack by a hydroxyl group generated from water by a histidine on the opposite side of the active site (Fig. 8). A hydroxyl nucleophile generated by His247-mediated deprotonation of water most likely facilitates hydrolysis in this geometry because His247 is 3.5 Å away from the carbonyl group and is in the same plane, while His278 is 0.5 Å farther from the carbonyl group and ~45 deg off axis compared with His247 (Fig. 6). Similar to the previously established model of VanX,[35] hydrolytic cleavage of the peptide bond occurs after the formation of a tetrahedral intermediate, which forms a bidentate complex with Zn^{2+} (Fig. 8, step 3). gp13-His247 is homologous to LytM-His260, Ale-1-His200, lysostaphin-His225,[23,48] and MepA-His206 (structural superposition not shown).

gp13-like enzymes in other phages

Other phages encode gp13/lysostaphin-like enzymes that may reflect parallel evolution of PG cross-link-cleaving Zn^{2+} metallopeptidases. The lactococcal phages and ϕ29 family members share

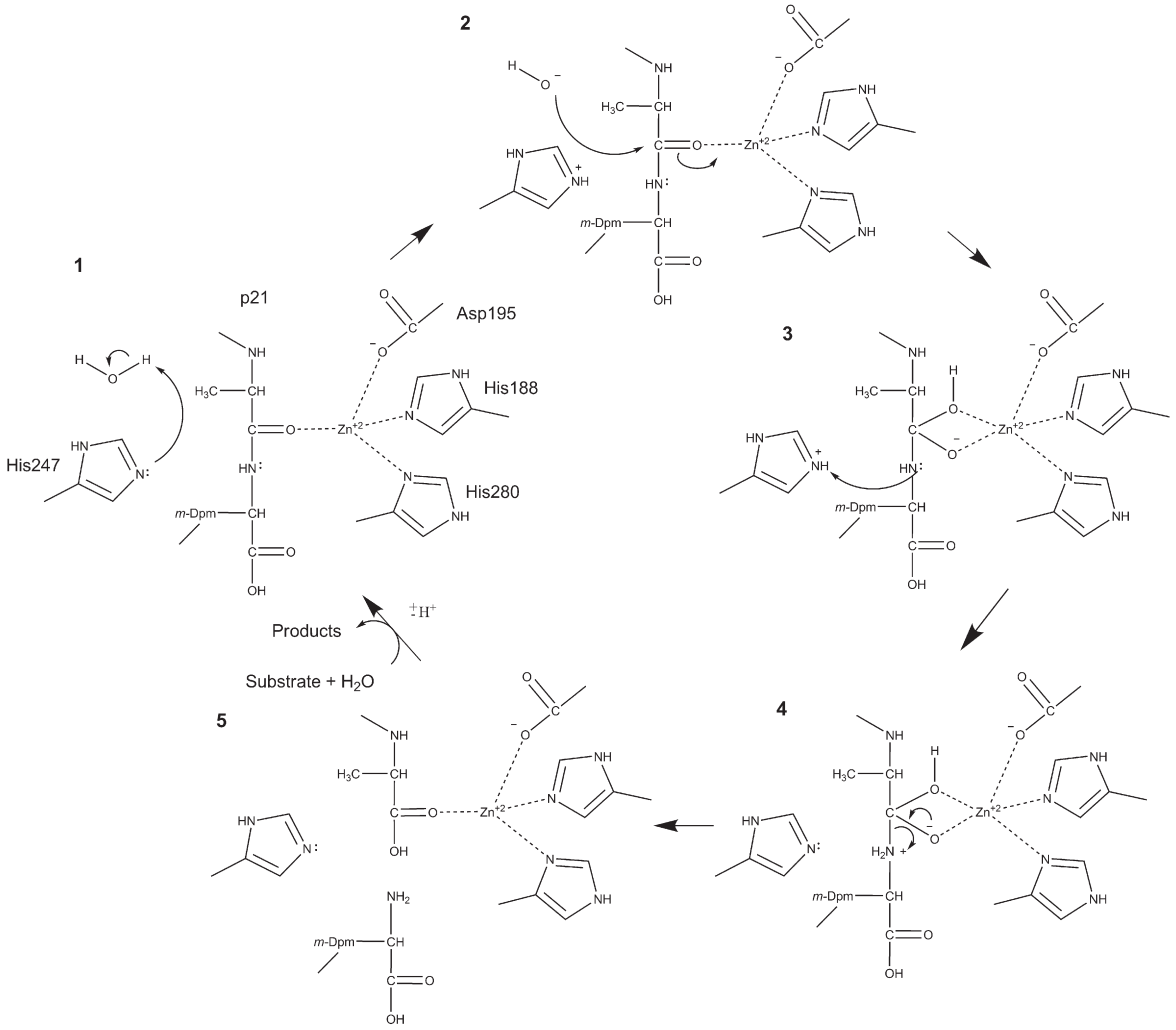

Fig. 8. Proposed hydrolysis reaction of the *B. subtilis* PG cross-link p21 catalyzed by the bacteriophage ϕ29 gp13. Step 1:substrate binding to the gp13 active-site with Asp195-mediated polarization of the scissile-bond carbonyl carbon and deprotonation of water. Step 2:hydroxyl nucleophile attack of the scissile-bond carbon leading to the bidentate complex and tetrahedral intermediate. Step 3:proton removal from His247 by the lone pair on the nitrogen of the scissile bond. Step 4:hydrolysis. Step 5:product release.

the His-x(3,6)-Asp and His-x-His motifs (Fig. 5). As infection by the 10^{31} phages[49] is a frequent genetic transfer event, the likelihood of parallel evolution of entry mechanisms of different phages in conjunction with possible lateral gene transfer from the host warrants further investigation.

Methods

Phage and protein preparation

Phage ϕ29 with wt gp13 was prepared using the delayed-lysis fiberless mutant *sus*8.5(900)14(1241) as described previously.[23] The gp13 NTD, CTD, full-length, and aspartate 195 mutant gp13 proteins were expressed in either Codon Plus (Strategene) or Rosetta (Novagen) strains as previously described,[31] with modifications. A cocktail of metals (1 μM $ZnCl_2$, 0.5 μM $MnCl_2$, and 0.37 μM $CoCl_2$) was modified from prior work[50] and included in the induction medium. Ethylenediaminetetraacetic acid (EDTA) was omitted from all buffers and protease inhibitors. The gp13 CTD and the D195A and D195C mutants were expressed in Rosetta. Cells (OD_{600} = 0.5, Klett = 44) were grown from overnight cultures with chloramphenicol (34 μg/mL) and ampicillin (100 μg/mL) to select for the Rosetta plasmid and the pTYB1 plasmid, respectively. Cultures were chilled to 0 °C in a water/ice bath for 5 min prior to IPTG induction at 1 mM and incubated at 20 °C overnight in a shaking water bath. Cells harvested by centrifugation were resuspended in 1/20 of the original volume of HST [20 mM Hepes, 500 mM NaCl, and 0.1% (v/v) Triton X-100, 4 °C] modified from the manufacturer's guidelines (NEB, Ipswich, MA) to omit the Zn^{2+}-chelating agent EDTA, washed of residual media, and resuspended in 30 mL of HST with an EDTA-free protease inhibitor mixture (Complete Mini EDTA-free, Roche, Indianapolis, IN) as per the manufacturer's recommendations (one tablet per 10 mL of concentrated cells). The cell concentrate was lysed by two or three passages through a chilled French press and checked for lysis by phase-contrast microscopy. The crude lysate was clarified by centrifugation at 4 °C, loaded onto a pre-HST buffer-equilibrated chitin–resin column (5–8 mL; NEB) at 4 °C, and run at a

flow rate not exceeding 0.5 mL/min. Self-cleavage of the intein fusion was induced, after a 20-column-volume HST wash to remove nonspecifically bound material, with HST + 50 mM DTT by room temperature incubation for 36–48 h. HST elution with 10 column volumes permitted sufficient protein recovery for subsequent concentration by Centriprep filters (molecular mass cutoff = 30 kDa; Millipore). Dialysis against TS (20 mM Tris, pH 7.4, and 150 mM NaCl) buffer was performed with a Slide-a-Lyzer (molecular mass cutoff = 10 kDa; Pierce) at 4 °C with two 1-L exchanges over 4–8 h each. Concentrated and buffer-exchanged protein was cryo-protected with the addition of sterile glycerol to 10% final concentration and stored at −80 °C. The protein was quantified by SDS-PAGE densitometry with bovine serum albumin standards.

Pfu polymerase (Stratagene) was used in circular PCR to generate the D195A and D195C mutants by modifying the full-length gp13 plasmid pTYB1[31] using standard conditions and primers as follows:

gp13 D195A forward primer 5′GGAACACTTTGTATA**GCC**-TTTGTGGGCAAAACTGAAAAGTACCC3′;
gp13 D195A reverse primer 5′GGGTACTTTTCAGTTTTGCC-CACAAA**GGC**TATACAAAGTGTTCC3′;
gp13 D195C forward primer 5′GGAACACTTTGTATA**TGC**-TTTGTGGGCAAAACTGAAAAGTACCC3′; and
gp13 D195C reverse primer 5′GGGTACTTTTCAGTTTTGCC-CACAAA**GCA**TATACAAAGTGTTCC3′.

PG purification and HPLC analysis

PG from vegetative *B. subtilis* cells was purified and digested with muramidase (Mutanolysin, Sigma-Aldrich) as previously described.[12] Muropeptides were reduced with borohydride and separated by HPLC using a $NaPO_4$ buffer and a methanol gradient as described previously.[12,51] Muropeptides in enzyme assay samples were analyzed using the same HPLC system without borohydride reduction. Muropeptides to be purified for use as substrates in enzymatic assays or for structural analyses were further purified using HPLC and a trifluoroacetic acid–acetonitrile buffer system.[32] The structures of purified muropeptides were verified using amino acid analysis[52] and mass spectrometry[53] as previously described. Muropeptides (250 pM) were incubated with gp13 (100 pM) in TS (20 mM Tris, pH 7.4, and 150 mM NaCl) buffer for 3 h at 37 °C, and the reaction was halted by acidification with phosphoric acid added to 5% (v/v). Chromatograms were analyzed using PowerChrom (eDaq, Colorado Springs, CO). The raw peak areas were converted to molar equivalence to p3 using calculated extinction coefficients[54] for muropeptides (p21, p3, p7) and then normalized to mole fraction of total area per run.

Amino acid analysis

Purified putative p7 muropeptide was either modified by FDNB or left untreated. Samples in 0.1 M $NaHCO_3$ were incubated with 16 mM FDNB for 16 h at room temperature in the dark. Both samples were then dried, acid hydrolyzed, and subjected to amino acid analysis as previously described.[52]

Computational modeling

All modeling and atomic distance measurements were done with the X-ray crystallographic structure of gp13[31] using Maestro (Schrödinger, LLC, New York, NY; 2007). The fragment model of the *B. subtilis* cross-link was built and energy minimized using the OPLS 2005 force field. The docking of the modeled fragment was carried out using the well-validated[55] and widely used Glide (Schrödinger, LLC; 2007) with default extra precision parameters. The Zn^{2+} ion, His247, and His278 side chains were defined as potential hydrogen-bond donor/acceptor constraints for the docking.

Spectroscopy

CD spectra of gp13 and the mutant proteins D195A and D195C (0.1 mg/mL) were conducted from 195 to 260 nm at a data pitch of 0.1 nm, acquiring 100 nm/min, with 4-s response and 1-nm bandwidth using a 0.1-cm cuvette in a Jasco 815. Five measurements were accumulated per sample. Purified proteins were dialyzed against 10 mM potassium phosphate, pH 7.4, buffer using 10-kDa microdialysis cups (Pierce). Protein concentration was assayed by SDS-PAGE densitometry with bovine serum albumin standards.

PIXE was conducted with acetone-precipitated protein (400 μg) and filter collected on 1-cm^2 nylon membranes (Boehringer Mannheim). Briefly, samples were mixed with −20 °C acetone to 80% acetone (v/v) and incubated at −20 °C for 10 min. Visible precipitates were present. Nylon filters with 80% acetone-washed samples and dried for at least 10 h at 25 °C were analyzed using a 1.7-MeV Pelletron accelerator (National Electrostatic Corporation) configured to generate a 4.0-MeV He^{++} ion beam at a beam current of ~30 nA in a circular beam 1.5–2 mm in diameter. Sample-emitted X-rays were counted and energy analyzed using a Kevex Si(Li) X-ray detector with 5-mm Be window and an energy resolution of 145 eV; a capping Al foil was also used to reduce the photon flux to the detector to prevent pile-up. PIXE spectra were acquired using the Hypra program (Charles Evans and Associates) during a dose of 40 or 20 μC, summed to a total of 80 μC per sample. The Zn $K\alpha_{1,2}$ (8.63 keV) line intensity was used to detect and gauge Zn content.

Sequence alignment

Sequence alignment of LytM (GI:87160448) and gp13 homologs in ϕ29 family members [ϕ29 (GI:137932), GA-1 (GI:12248120), and B103 (GI:2285516)] was conducted using ClustalW within AlignX of the Vector NTI suite (v.10, Invitrogen, Carlsbad, CA). Lactococcal phage-related proteins were identified by an ACLAME[56,57] search using gp13. The proteins include bIL285 endopeptidase (GI:13095734), TP901-1 "ORF47" (GI:13786578), Tuc2009 "minor structural protein 3" (GI:13487849), and ul36 "structural protein" (GI:21716123). The alignments to lactococcal phages were added to the gp13–LytM alignment and displayed using AlignX.

Acknowledgements

D.N.C., Y.Y.S., G.D.H., D.L.A., and D.L.P. designed the experiments, while D.N.C., Y.Y.S., G.D.H., and D.L.P. performed them. D.N.C., Y.Y.S., G.D.H., D.L.A., and D.L.P. analyzed the data. Y.X. and M.G.R. provided the gp13 plasmid and the purified

N-terminal protein used in this study. D.N.C., Y.Y.S., D.L.A., and D.L.P. wrote the article. This work was supported by the National Institutes of Health through grant DE003606 (to D.L.A.) from the National Institute of Dental and Craniofacial Research and grant GM056695 (to D.L.P.) from the National Institute of General Medical Sciences. The content is solely the responsibility of the authors and does not necessarily represent the official views of the National Institute of Dental and Craniofacial Research, the National Institute of General Medical Sciences, or the National Institutes of Health. We thank Dr. John Lipscomb for critical reading of previous versions of the manuscript and Dr. Matthias Bochtler for helpful discussion. We also thank Jessica McElligott for technical assistance and the University of Minnesota Supercomputing Institute for providing the computational resource for the molecular modeling study as well as the Characterization Facility (which receives partial support from the National Science Foundation through the National Nanotechnology Infrastructure Network program) for providing the ion beam analysis resources.

Supplementary Data

Supplementary data associated with this article can be found, in the online version, at doi:10.1016/j.jmb.2009.02.001

References

1. Rossmann, M. G., Mesyanzhinov, V. V., Arisaka, F. & Leiman, P. G. (2004). The bacteriophage T4 DNA injection machine. *Curr. Opin. Struct. Biol.* **14**, 171–180.
2. Kanamaru, S., Ishiwata, Y., Suzuki, T., Rossmann, M. G. & Arisaka, F. (2005). Control of bacteriophage T4 tail lysozyme activity during the infection process. *J. Mol. Biol.* **346**, 1013–1020.
3. Andrews, D., Butler, J. S., Al-Bassam, J., Joss, L., Winn-Stapley, D. A., Casjens, S. & Cingolani, G. (2005). Bacteriophage P22 tail accessory factor gp26 is a long triple-stranded coiled-coil. *J. Biol. Chem.* **280**, 5929–5933.
4. Meijer, W. J., Horcajadas, J. A. & Salas, M. (2001). ϕ29 family of phages. *Microbiol. Mol. Biol. Rev.* **65**, 261–287.
5. Leiman, P. G., Battisti, A. J., Bowman, V. D., Stummeyer, K., Muhlenhoff, M., Gerardy-Schahn, R. *et al.* (2007). The structures of bacteriophages K1E and K1-5 explain processive degradation of polysaccharide capsules and evolution of new host specificities. *J. Mol. Biol.* **371**, 836–849.
6. Iwashita, S. & Kanegasaki, S. (1973). Smooth specific phage adsorption: endorhamnosidase activity of tail parts of P22. *Biochem. Biophys. Res. Commun.* **55**, 403–409.
7. Rydman, P. S. & Bamford, D. H. (2000). Bacteriophage PRD1 DNA entry uses a viral membrane-associated transglycosylase activity. *Mol. Microbiol.* **37**, 356–363.
8. Mosig, G., Lin, G. W., Franklin, J. & Fan, W. H. (1989). Functional relationships and structural determinants of two bacteriophage T4 lysozymes: a soluble (gene e) and a baseplate-associated (gene 5) protein. *New Biol.* **1**, 171–179.
9. Boulanger, P., Jacquot, P., Plancon, L., Chami, M., Engel, A., Parquet, C. *et al.* (2008). Phage T5 straight tail fiber is a multifunctional protein acting as a tape measure and carrying fusogenic and muralytic activities. *J. Biol. Chem.* **283**, 13556–13564.
10. Moak, M. & Molineux, I. J. (2000). Role of the gp16 lytic transglycosylase motif in bacteriophage T7 virions at the initiation of infection. *Mol. Microbiol.* **37**, 345–355.
11. Molineux, I. J. (2006). The T7 group. In *The Bacteriophages* (Calendar, R., ed), 2nd edit., pp. 277–301, Oxford University Press, New York, NY.
12. Atrih, A., Bacher, G., Allmaier, G., Williamson, M. P. & Foster, S. J. (1999). Analysis of peptidoglycan structure from vegetative cells of *Bacillus subtilis* 168 and role of PBP 5 in peptidoglycan maturation. *J. Bacteriol.* **181**, 3956–3966.
13. Odintsov, S. G., Sabala, I., Marcyjaniak, M. & Bochtler, M. (2004). Latent LytM at 1.3 Å resolution. *J. Mol. Biol.* **335**, 775–785.
14. Firczuk, M., Mucha, A. & Bochtler, M. (2005). Crystal structures of active LytM. *J. Mol. Biol.* **354**, 578–590.
15. Surovtsev, V. I., Fedorov, T. V. & Borozdina, M. A. (2004). Michaelis–Menten kinetics for determining enzymatic activity of lysostaphin. *Biochemistry (Moscow)*, **69**, 754–756.
16. Browder, H. P., Zygmunt, W. A., Young, J. R. & Tavormina, P. A. (1965). Lysostaphin: enzymatic mode of action. *Biochem. Biophys. Res. Commun.* **19**, 383–389.
17. Schindler, C. A. & Schuhardt, V. T. (1964). Lysostaphin: a new bacteriolytic agent for the Staphylococcus. *Proc. Natl Acad. Sci. USA*, **51**, 414–421.
18. Quinn, E. L., Jones, D. N., Steinhauer, B. W. & Cox, F. (1966). *In vitro* activity of lysostaphin. *Antimicrob. Agents Chemother. (Bethesda)*, **6**, 382–388.
19. Kline, S. A., de la Harpe, J. & Blackburn, P. (1994). A colorimetric microtiter plate assay for lysostaphin using a hexaglycine substrate. *Anal. Biochem.* **217**, 329–331.
20. Bochtler, M., Odintsov, S. G., Marcyjaniak, M. & Sabala, I. (2004). Similar active sites in lysostaphins and D-Ala-D-Ala metallopeptidases. *Protein Sci.* **13**, 854–861.
21. Lu, J. Z., Fujiwara, T., Komatsuzawa, H., Sugai, M. & Sakon, J. (2006). Cell wall-targeting domain of glycyl-glycine endopeptidase distinguishes among peptidoglycan cross-bridges. *J. Biol. Chem.* **281**, 549–558.
22. Marcyjaniak, M., Odintsov, S. G., Sabala, I. & Bochtler, M. (2004). Peptidoglycan amidase MepA is a LAS metallopeptidase. *J. Biol. Chem.* **279**, 43982–43989.
23. Cohen, D. N., Erickson, S. E., Xiang, Y., Rossmann, M. G. & Anderson, D. L. (2008). Multifunctional roles of a bacteriophage ϕ29 morphogenetic factor in assembly and infection. *J. Mol. Biol.* **378**, 804–817.
24. Kenny, J. G., McGrath, S., Fitzgerald, G. F. & van Sinderen, D. (2004). Bacteriophage Tuc2009 encodes a tail-associated cell wall-degrading activity. *J. Bacteriol.* **186**, 3480–3491.
25. Anderson, D. L. & Reilly, B. E. (1993). Morphogenesis of bacteriophage ϕ29. In *Bacillus subtilis and Other Gram-Positive Bacteria: Biochemistry, Physiology, and Molecular Genetics* (Sonenshein, A. L., Hoch, J. A. & Losick, R., eds), 2nd edit., pp. 859–867, American Society for Microbiology, Washington, DC.
26. Grimes, S., Jardine, P. J. & Anderson, D. (2002). Bacteriophage ϕ29 DNA packaging. *Adv. Virus Res.* **58**, 255–294.
27. Young, F. E. (1967). Requirement of glucosylated teichoic acid for adsorption of phage in *Bacillus subtilis* 168. *Proc. Natl Acad. Sci. USA*, **58**, 2377–2384.

28. Young, F. E., Smith, C. & Reilly, B. E. (1969). Chromosomal location of genes regulating resistance to bacteriophage in *Bacillus subtilis*. *J. Bacteriol.* **98**, 1087–1097.
29. Tosi, M. E., Reilly, B. E. & Anderson, D. L. (1975). Morphogenesis of bacteriophage ϕ29 of *Bacillus subtilis*: cleavage and assembly of the neck appendage protein. *J. Virol.* **16**, 1282–1295.
30. Garcia, J. A., Carrascosa, J. L. & Salas, M. (1983). Assembly of the tail protein of the *Bacillus subtilis* phage ϕ29. *Virology*, **125**, 18–30.
31. Xiang, Y., Morais, M. C., Cohen, D. N., Bowman, V. D., Anderson, D. L. & Rossmann, M. G. (2008). Crystal and cryoEM structural studies of a cell-wall degrading enzyme in the bacteriophage ϕ29 tail. *Proc. Natl Acad. Sci. USA*, **105**, 9552–9557.
32. Popham, D. L., Helin, J., Costello, C. E. & Setlow, P. (1996). Analysis of the peptidoglycan structure of *Bacillus subtilis* endospores. *J. Bacteriol.* **178**, 6451–6458.
33. Baxa, U., Steinbacher, S., Miller, S., Weintraub, A., Huber, R. & Seckler, R. (1996). Interactions of phage P22 tails with their cellular receptor, *Salmonella* O-antigen polysaccharide. *Biophys. J.* **71**, 2040–2048.
34. Gasteiger, E., Hoogland, C., Gattiker, A., Duvaud, S., Wilkins, M. R., Appel, R. D. & Bairoch, A. (2005). Protein identification and analysis tools on the ExPASy server. In *The Proteomics Protocols Handbook* (Walker, J. M., ed), pp. 571–607, Humana Press, Totowa, NJ.
35. Bussiere, D. E., Pratt, S. D., Katz, L., Severin, J. M., Holzman, T. & Park, C. H. (1998). The structure of VanX reveals a novel amino-dipeptidase involved in mediating transposon-based vancomycin resistance. *Mol. Cell*, **2**, 75–84.
36. Trzaskowski, B., Adamowicz, L. & Deymier, P. (2008). A theoretical study of zinc(II) interactions with amino acid models and peptide fragments. *J. Biol. Inorg. Chem.* **13**, 133–137.
37. Firczuk, M. & Bochtler, M. (2007). Mutational analysis of peptidoglycan amidase MepA. *Biochemistry (NY)*, **46**, 120–128.
38. Hagen, E. W., Reilly, B. E., Tosi, M. E. & Anderson, D. L. (1976). Analysis of gene function of bacteriophage ϕ29 of *Bacillus subtilis*: identification of cistrons essential for viral assembly. *J. Virol.* **19**, 501–517.
39. Lai, A. C., Tran, S. & Simmonds, R. S. (2002). Functional characterization of domains found within a lytic enzyme produced by *Streptococcus equi* subsp. *zooepidemicus*. *FEMS Microbiol. Lett.* **215**, 133–138.
40. Pritchard, D. G., Dong, S., Baker, J. R. & Engler, J. A. (2004). The bifunctional peptidoglycan lysin of *Streptococcus agalactiae* bacteriophage B30. *Microbiology*, **150**, 2079–2087.
41. Navarre, W. W., Ton-That, H., Faull, K. F. & Schneewind, O. (1999). Multiple enzymatic activities of the murein hydrolase from staphylococcal phage ϕ11. Identification of a D-alanyl-glycine endopeptidase activity. *J. Biol. Chem.* **274**, 15847–15856.
42. Xiang, Y., Morais, M. C., Battisti, A. J., Grimes, S., Jardine, P. J., Anderson, D. L. & Rossmann, M. G. (2006). Structural changes of bacteriophage ϕ29 upon DNA packaging and release. *EMBO J.* **25**, 5229–5239.
43. Smith, D. E., Tans, S. J., Smith, S. B., Grimes, S., Anderson, D. L. & Bustamante, C. (2001). The bacteriophage ϕ29 portal motor can package DNA against a large internal force. *Nature*, **413**, 748–752.
44. Rickgauer, J. P., Fuller, D. N., Grimes, S., Jardine, P. J., Anderson, D. L. & Smith, D. E. (2008). Portal motor velocity and capsid pressure during viral DNA packaging in bacteriophage ϕ29. *Biophys. J.* **94**, 159–167.
45. Gonzalez-Huici, V., Salas, M. & Hermoso, J. M. (2004). The push–pull mechanism of bacteriophage ϕ29 DNA injection. *Mol. Microbiol.* **52**, 529–540.
46. Ramadurai, L., Lockwood, K. J., Nadakavukaren, M. J. & Jayaswal, R. K. (1999). Characterization of a chromosomally encoded glycylglycine endopeptidase of *Staphylococcus aureus*. *Microbiology*, **145**, 801–808.
47. Fujiwara, T., Aoki, S., Komatsuzawa, H., Nishida, T., Ohara, M., Suginaka, H. & Sugai, M. (2005). Mutation analysis of the histidine residues in the glycylglycine endopeptidase ALE-1. *J. Bacteriol.* **187**, 480–487.
48. Ramadurai, L. & Jayaswal, R. (1997). Molecular cloning, sequencing, and expression of lytM, a unique autolytic gene of *Staphylococcus aureus*. *J. Bacteriol.* **179**, 3625–3631.
49. Hendrix, R. W., Smith, M. C., Burns, R. N., Ford, M. E. & Hatfull, G. F. (1999). Evolutionary relationships among diverse bacteriophages and prophages: all the world's a phage. *Proc. Natl Acad. Sci. USA*, **96**, 2192–2197.
50. Hoffman, B. J., Broadwater, J. A., Johnson, P., Harper, J., Fox, B. G. & Kenealy, W. R. (1995). Lactose fed-batch overexpression of recombinant metalloproteins in *Escherichia coli* BL21(DE3): process control yielding high levels of metal-incorporated, soluble protein. *Protein Expression Purif.* **6**, 646–654.
51. McPherson, D. C. & Popham, D. L. (2003). Peptidoglycan synthesis in the absence of class A penicillin-binding proteins in *Bacillus subtilis*. *J. Bacteriol.* **185**, 1423–1431.
52. González-Castro, M. J., López-Hernández, J., Simal-Lozano, J. & Oruña-Concha, M. J. (1997). Determination of amino acids in green beans by derivatization with phenylisothiocianate and high-performance liquid chromatography with ultraviolet detection. *J. Chromatogr. Sci.* **35**, 181–185.
53. Orsburn, B., Melville, S. B. & Popham, D. L. (2008). Factors contributing to heat resistance of *Clostridium perfringens* endospores. *Appl. Environ. Microbiol.* **74**, 3328–3335.
54. Glauner, B. (1988). Separation and quantification of muropeptides with high-performance liquid chromatography. *Anal. Biochem.* **172**, 451–464.
55. Kontoyianni, M., McClellan, L. M. & Sokol, G. S. (2004). Evaluation of docking performance: comparative data on docking algorithms. *J. Med. Chem.* **47**, 558–565.
56. Leplae, R., Hebrant, A., Wodak, S. J. & Toussaint, A. (2004). ACLAME: A CLAssification of Mobile genetic Elements. *Nucleic Acids Res.* **32**, D45–D49.
57. Toussaint, A., Lima-Mendez, G. & Leplae, R. (2007). PhiGO, a phage ontology associated with the ACLAME database. *Res. Microbiol.* **158**, 567–571.